

Spatio-temporal Weather Forecasting and Attention Mechanism on Convolutional LSTMs

Selim Furkan Tekin, Oguzhan Karaahmetoglu, Fatih Ilhan, Ismail Balaban and Suleyman S. Kozat, *Senior Member*

Abstract—Numerical weather forecasting on high-resolution physical models consume hours of computations on supercomputers. Application of deep learning and machine learning methods in forecasting revealed new solutions in this area. In this paper, we forecast high-resolution numeric weather data using both input weather data and observations by providing a novel deep learning architecture. We formulate the problem as spatio-temporal prediction. Our model is composed of *Convolutional Long-short Term Memory*, and *Convolutional Neural Network* units with *encoder-decoder* structure. We enhance the short-long term performance and interpretability with an attention and a context matcher mechanism. We perform experiments on high-scale, real-life, benchmark numerical weather dataset, *ERA5 hourly data on pressure levels*, and forecast the temperature. The results show significant improvements in capturing both spatial and temporal correlations with attention matrices focusing on different parts of the input series. Our model obtains the best validation and the best test score among the baseline models, including ConvLSTM forecasting network and U-Net. We provide qualitative and quantitative results and show that our model forecasts 10 time steps with 3 hour frequency with an average of 2 degrees error. Our code and the data are publicly available.

Index Terms—spatio-temporal, weather, forecasting, attention.

I. INTRODUCTION

A. Preliminaries

WEATHER affects people's daily lives and changes their decisions since the beginning of humanity. The weather molds the flow of events and creates a snowballing effect on real-life systems such as agriculture, tourism, traffic, flight navigation, and energy consumption. In these topics, the data scientists try to predict their system's next state, where the weather becomes a critical information to estimate. With the success of modelling spatio-temporal series [1]–[6], data scientists create new deep-learning-based solutions to the weather forecasting, which have many advantages over traditional methods. Compared to physical models for *Numerical Weather Prediction* (NWP), deep learning models can provide results within the minutes of receiving data, exploit the big data aggregated in years, and make accurate predictions with less costly models. This paper introduces a model architecture for the NWP by combining multiple spatio-temporal data sources with an attention mechanism and using *Convolutional*

Selim Furkan Tekin, Oguzhan Karaahmetoglu, Fatih Ilhan and Suleyman S. Kozat are with the Department of Electrical and Electronics Engineering, Bilkent University, Bilkent, Ankara 06800, Turkey e-mail: {tekin; koguzhan; filhan; kozat}@ee.bilkent.edu.tr

Ismail Balaban is with the Department of Informatics, Middle East Technical University, METU, Ankara 06800, Turkey e-mail: ismail.balaban@metu.edu.tr

Long-short Term Memory (ConvLSTM) [7] cells as building blocks to capture spatial and temporal correlations. Our model can select relevant cells in multiple spatio-temporal series to make long term spatial predictions by preserving long term dependencies with attention and context matcher mechanisms. Further, we give a weather prediction pipeline for short-middle-long term predictions, and our code and data are available at https://github.com/sftekin/ieee_weather.

Today's traditional NWP methods model atmospheric events using physics, which is first introduced in the early twentieth century [8]. NWP models simulate the underlying physics of atmosphere by solving non-linear partial differential equations at millions of points per time stamp and providing reliable forecasts. Daily simulations run on NWP can forecast minutes to weeks ahead for regions with meter to kilometer resolutions [9]. However, numerical models are getting more complex, and their demand for high computation power increases day by day. Obtaining results from these models can take hours of waiting, limiting their ability to provide actionable predictions. For example, Turkish State Meteorological Service uses supercomputers to upsample large-scale NWPs such as [10]–[13] to local regions. However, with deep learning models, one can obtain local predictions with fewer computations.

The NWP is a multiple time series problem and classical ML algorithms have shown great success in time series applications. In [14], authors successfully train Neural Networks (NNs) for energy forecasting of each zone. Likewise, authors of [15] formulated Recurrent Neural Network (RNN) and Convolutional Neural Network (CNN) under multistep and recursive manners and showed great success compared to statistical models. In a more challenging task of forecasting non-stationary time series data, authors of [16] combine statistical method and deep learning models to forecast the M4 dataset. Moreover, with the development of new methods on time series prediction, one can combine multiple time series with attention mechanisms, [17], or perform dilated causal convolutions in time, [18], [19], to generate accurate long term predictions. However, all of these methods focused on the next value of the one target series. In [20], authors predict multiple time series using covariates of multiple input series. In the spatio-temporal time series prediction, however, there are multiple series to predict, which have both temporal and spatial covariances.

Furthermore, previous studies on spatio-temporal series [21]–[23], including ConvLSTMS, do not exploit the numerous data set available for weather, such as satellite images, numerical grid values, and observations in meteorological stations. These works have focused on the precipitation now-

casting problem, where this task aims to give a precise and timely prediction of rainfall intensity in a local region over a relatively short period [7]. The inputs and outputs are a sequence of radar images, which makes an image translation problem rather than a time series problem, and it focused on one source of data. The weather, however, is a chaotic system affected by many parameters, e.g., vegetation, geographical contour, and human factors. Thus, less amount of information is not enough to model such chaotic behaviours. Besides, [7], [21]–[23], made accurate short-term predictions, yet their performance deteriorated rapidly as the output sequence length raises.

Additionally, we show that classical side information integration in computer vision [24]–[26] or in spatio-temporal forecasting [26], [27] does not apply to NWP with ConvLSTMs. We confirm that any unnormalized non-positive multiplication operation, including creating embeddings with NNs or CNNs, create perturbations on the natural flow, which changes both spatial and temporal covariances. Moreover, we show that the natural flows are preserved with the convolutional attention mechanism.

To this end, we introduce attention based ConvLSTM encoder-decoder architecture with context matcher for spatio-temporal forecasting as shown in Figure 1. Input sequences first pass from the attention mechanism, where the model selects relevant driving series to make predictions by referring to the past encoder hidden state at each time step. The encoder block consists of stacked ConvLSTM units, which encode the input sequence of data to hidden states. In the second stage, the context-matcher mechanism matches the decoder’s hidden states by summing the encoder’s hidden states across all time steps to carry out the long-term dependencies by increasing the length of gradient flows. Each ConvLSTM unit in the decoder block, decodes the passed information from the hidden layers of the encoder. Output of the decoder then passes through the output convolutions to produce predictions. The architecture provides selection on input time series from extracted spatial features and capture long term dependencies. We call the architecture as *Weather Model*. We demonstrate significant performance gains through an extensive set of experiments compared to the conventional methods and show that the weather model is easy to interpret.

B. Prior Art and Comparisons

The application of deep learning methods to weather forecasting is an extensively studied area. We can divide the works into two by the ones that predict single and the ones that predict multiple time-series.

For the single time-series forecasting, [28] leveraged a massive volume of weather dataset to train Auto-encoder with Deep Neural Network (DNNs) to simulate hourly weather data and learn features. [29], improved this approach by introducing stacked auto-encoders to temperature forecasting with corrupted inputs by noise. A review [30] compared the NN, CNN, and Conditional Restricted Boltzmann Machine performances. Further, [31] implemented simple NN using different climate indices from different stations and historical

rainfall data to forecast rainfall. These works showed the high performance of simple deep learning architectures when used with a high volume of data. For the severe convective weather event prediction, [32] showed the success of deep CNNs, in classifying atmospheric data from multiple pressure levels. Moreover, Recurrent Neural Network (RNN) [33] and Long-short Term Memory (LSTM) [34] applied for the weather forecasting and [35] focused on the vanishing gradient problem by implementing intensified LSTM architecture for rainfall forecasting. [36] introduced Deep uncertainty quantification, which uses RNN based architecture to single-value forecast and uncertainty quantification. Recently, [37] used Temporal Convolutional Network (TCN) for multiple-output and single-output weather predictions and showed better results than a physical NWP model, WRF [10]. However, this approach is costly and did not incorporate the multiple features and spatial covariances and showed high performance on multiple-inputs and single-output models.

We categorized the works on video forecasting and precipitation nowcasting as the multiple time-series prediction. [7] introduced the ConvLSTM model with the forecasting network, which consists of an encoder and a decoder built by stacked ConvLSTMs. This model can capture the spatial-temporal covariances and showed high performance in moving the MNIST dataset and predicting a region’s rainfall intensity. Also, [38] used this architecture to track hurricanes. Later, [21] introduced Trajectory Gated Recurrent Unit (Traj-GRU) to learn location invariant movements between input radar images and showed higher performance compared to [7] and optical flow networks [23]. However, the proposed network architectures in [7] and [21] must take a one-dimensional tensor to predict one-dimensional output. Further, [39] improved the forecasting architecture by the downsampling and the upsampling layers between TrajGRU units and output convolutions omits the problem of multidimensional input. [40] introduced the recursive prediction of decoder in the forecasting architecture. To solve this architecture’s blurred outputs caused by MSE, [41] implemented Generative Adversarial Neural Network with different loss. Besides, U-Net showed high performance on precipitation nowcasting in [42], which is comparable with ConvLSTMs.

Attention mechanisms in the spatio-temporal domain are studied in various tasks. For the human action recognition, [43] developed temporal and spatial attention mechanism with fully connected NNs and LSTMs. Likewise, [17] implemented a dual attention mechanism in time-series forecasting. [27] implemented a multi-level attention mechanism fusing side-information with multiple geo-sensory time-series data to forecast air quality. For the traffic prediction, [44] implemented an attention mechanism to the outputs of LSTM, which takes inputs from different past periods. Although these works successfully implement attention mechanism, input is single or multiple time-series rather than 3D tensors. The authors of [45] implement an attention mechanism to improve ConvLSTM further, which takes 3D tensors as input; however, the performance increased scarcely. Recently, [46] CNN following LSTM (Conv + LSTM) with ConvLSTM in temporally unrolled architecture and temporally concatenated

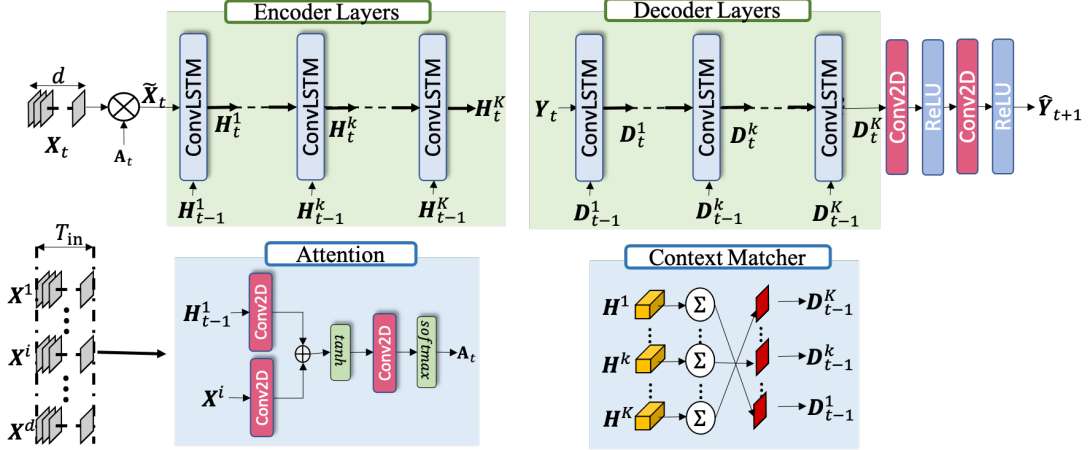


Fig. 1: Graph of *Weather Model*. Each time instance of the spatio-temporal input series $\mathbf{X}_t = \{\mathbf{X}_t^1, \dots, \mathbf{X}_t^i, \dots, \mathbf{X}_t^d\}$ first multiplied by the attention matrices $\mathbf{A}_t = (\mathbf{A}_t^1, \dots, \mathbf{A}_t^i, \dots, \mathbf{A}_t^d)$ to create $\tilde{\mathbf{X}}_t = (\mathbf{X}_t^1 \cdot \mathbf{A}_t^1, \dots, \mathbf{X}_t^i \cdot \mathbf{A}_t^i, \dots, \mathbf{X}_t^d \cdot \mathbf{A}_t^d)$. The attention mechanism computes the attention weights \mathbf{A}_t^i for extracted feature conditioned on first layer of previous hidden state \mathbf{H}_{t-1}^1 of encoder. Weighted inputs for each time step, $\tilde{\mathbf{X}}_t$, feeds to the ConvLSTM unit of the first layer of the encoder, where $\tilde{\mathbf{X}}_t^i \in \mathbb{R}^{M \times N \times d}$. After the input sequence has passed from the encoder layers, the encoder’s hidden states, $\mathbf{H} = (\mathbf{H}^1, \dots, \mathbf{H}^k, \dots, \mathbf{H}^K)$, pass to Context Matcher, where each $\mathbf{H}^k = (\mathbf{H}_1^k, \dots, \mathbf{H}_t^k, \dots, \mathbf{H}_{T_{in}}^k)$. The Context Matcher sums the hidden states in time dimension and reverses the states layer order to create $\mathbf{D}_{t-1} = (\mathbf{D}_{t-1}^1, \dots, \mathbf{D}_{t-1}^k, \dots, \mathbf{D}_{t-1}^K)$. Final output of the final decoder layer, \mathbf{D}_t^K passes to output convolutions to create prediction $\hat{\mathbf{Y}}_{t+1}$.

architecture. They observed the loss change according to different inputs, e.g., features, locations to interpret the model decisions. Compared to Conv + LSTM, ConvLSTM showed high performance. However, they obtained interpretable results only for the Conv + LSTM model, and their interpretation is on feature and location level rather than the activations of the model.

Finally, [47] introduced a benchmark dataset, ERA5 [48], to predict global weather pattern days in advance. They provide baseline scores from simple linear regression techniques, deep learning models, and purely physical forecasting models.

C. Contributions

Our main contributions are as follows:

- We introduce attention-based recurrent network architecture to be used in spatio-temporal series with convolution operations on attention layers and ConvLSTMs as memory units. With this framework, we can improve long-term predictions of the encoder-decoder structure of ConvLSTMs and learn spatial correlations better.
- To the best of our knowledge, the first time in the literature, we apply an attention-based ConvLSTM network to spatio-temporal weather forecasting. This model architecture allows us to use multiple side-information and produce refined predictions with high interpretability.
- We show the performance decrease on ConvLSTMs with the traditional side information integration methods with the flow vectors.
- We present a pipeline for numerical weather forecasting. Even if the input series have different spatial and temporal resolutions, we can produce highly accurate predictions. Our code and the data are publicly available.

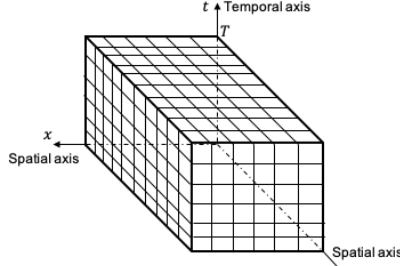
- We show that our framework can be used to combine different forecasts that can be results of NWP models and produce refined predictions as mixture of experts.
- Through an extensive set of experiments over real datasets, we demonstrate that our method brings significant improvements both long and short term predictions compared to state-of-the-art methods.

D. Organization

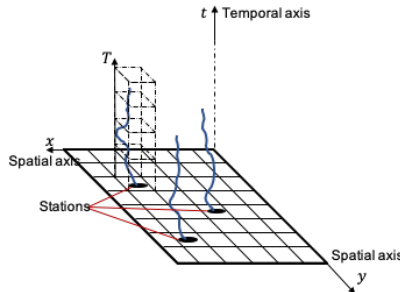
The remainder of the paper is organized as follows. In Section II, we define spatio-temporal weather forecasting and the introduce the interpolation method for the single time series of information. Next, we continue with describing model structure step by step in Section III. Then, in Section III-A, we describe the ConvLSTM unit and how it captures the spatial-temporal relationship in the data. We explain the encoder and the attention mechanism in Section III-B, and introduce the context matcher mechanism in Section III-C. Additionally, we describe the recursive prediction with Weather Model in the same section. In Section IV, we analyze our model’s performance over real datasets and compare with the baseline methods. In the same section we also provide some exploratory data analysis to our dataset. Lastly, we interpret Section IV’s results and conclude the paper in Section V with several remarks.

II. PROBLEM DESCRIPTION

In this paper, all vectors are column vectors and denoted by boldface lower case letters. Matrices and tensors are represented by boldface upper letters. For a vector \mathbf{a} , \mathbf{a}^T is ordinary transpose and $\|\mathbf{a}\| = \sqrt{\mathbf{a}^T \mathbf{a}}$ is the l^2 -norm. The time index is given subscript and upper-script refers to other signals,



(a) An example of spatio-temporal input sequence where T defines temporal window. At each time step t there is a spatial grid with area of xy . Each cell represents value of a region at time t .



(b) Illustration of weather data coming from stations located as points inside grid. This information is known as observational data. Meteorologists use this information for data assimilation of NWP models. In this paper, we interpolated these values to the target grid and used as one of the sources spatio-temporal input series.

Fig. 2: Illustrations of two type of meteorology data that is used in this paper.

e.g \mathbf{X}_i^k shows k^{th} input signal's i^{th} time step. Concatenation of two vectors is shown as brackets with semicolon e.g $[\mathbf{h}_t; \mathbf{s}_t]$.

This paper's primary goal is to forecast numeric weather data using multiple sources of historical numeric weather data. Mathematically the problem can be defined as follows: Multiple spatio-temporal series $\{\mathbf{X}^1, \dots, \mathbf{X}^k, \dots, \mathbf{X}^d\}$ enters to model where d is the number of series and each $\mathbf{X}^k \in \mathbb{R}^{M \times N \times T}$ where M and N defines spatial dimensions and T defines temporal dimension. An example spatio-temporal input is shown in Figure 2a. \mathbf{X}_i^k shows input series coming from source i at time t where $i \in \{t - T_{in}, \dots, t - T_{in} + j, \dots, t\}$. Likewise, the output of model can be described as \mathbf{Y}_i where $i \in \{t + j, \dots, t + T_{out}\}$. Every advance in time step t , is showed with j . Input series have same frequencies i.e input series will have $j = a \cdot f$ where f is the frequency of time series and $f, a \in \mathbb{Z}$. T_{in} and T_{out} show input and output temporal window sizes. Similarly, dimension of output tensor can be defined as $\mathbf{Y} \in \mathbb{R}^{M \times N \times T}$ and for any target value at time t , $\mathbf{Y}_t \in \mathbb{R}^{M \times N}$.

Another source of information is the observations coming from ground stations. These observations from station i are time series and can be represented as $\mathbf{x}^i \in \mathbb{R}^T$. Since our target series are spatio-temporal we interpolated this information by

Inverse Distance Weighting (IDW) [49] to the value cells in target grid. As shown in Figure 2b, there are multiple stations located in different cells, and we can represent the known values from stations as:

$$\{(\mathbf{x}^1, \mathbf{u}^1), (\mathbf{x}^2, \mathbf{u}^2), \dots, (\mathbf{x}^n, \mathbf{u}^n)\}$$

where, \mathbf{x}^i is the known value for the location $\mathbf{u}^i \in \mathbb{R}^2$ and $i = 1, 2, \dots, n$. The interpolated features for time t , can be represented as $\hat{x}_t = f(\hat{\mathbf{u}})$, where \hat{x}_t is the cell's interpolated value, $\hat{\mathbf{u}}$ is the cell's location, and $f(\cdot)$ is the IDW defined as,

$$f(\hat{\mathbf{u}}) = \begin{cases} \frac{\sum_{i=1}^n w_i(\hat{\mathbf{u}}) x_i^i}{\sum_{i=1}^n w_i(\hat{\mathbf{u}})} & d(\hat{\mathbf{u}}, \mathbf{u}_i) \neq 0 \\ x_t^i, & d(\hat{\mathbf{u}}, \mathbf{u}_i) = 0 \end{cases} \quad (1)$$

where the weight equation is:

$$w_i(\hat{\mathbf{u}}) = \frac{1}{d(\hat{\mathbf{u}}, \mathbf{u}_i)^p}$$

and the $d(\cdot)$ is the Haversine distance and the p is the power value which determines the strength of interpolation. If p value is too high, cells take the mean of the station values, and if it is too low, only the cells which are very close to stations will be interpolated. Thus, it is a critical parameter to select, and we implemented cross validation to find the p value for each t . Algorithm 1 shows the implementation of (1) and performing leave-one-out cross validation for each time step.

Algorithm 1 IDW Algorithm

```

 $\mathbf{X}^{\text{all}} \leftarrow \text{all\_station\_data}$ 
 $\mathbf{u} \leftarrow \text{station\_locations}$ 
 $\hat{\mathbf{u}} \leftarrow \text{cell\_locations}$ 
 $\mathbf{D} \leftarrow \text{calculate\_distance\_matrix}(\mathbf{u}, \hat{\mathbf{u}})$ 
 $\mathbf{P} \leftarrow \mathbf{0}$ 
 $t \leftarrow 0$ 
 $j \leftarrow 0$ 
for  $t \leq L$  do
  for  $j \leq d$  do
     $\mathbf{x}_{t,j} \leftarrow \mathbf{X}_{t,j}^{\text{all}}$ 
     $rmse \leftarrow \{\}$ 
    for  $p \in \text{power\_values}$  do
       $error \leftarrow 0$ 
       $i \leftarrow 0$ 
      for  $i \leq n$  do
         $x_{\text{validation}} \leftarrow \mathbf{x}_{t,j,i}$ 
         $\mathbf{x}_{\text{train}} \leftarrow \mathbf{x}_{t,j,i'}$ 
         $\mathbf{d}_{\text{train}} \leftarrow \mathbf{D}_i$ 
         $\mathbf{w} \leftarrow \mathbf{d}_{\text{train}}^{-p}$ 
         $\hat{x} \leftarrow (\mathbf{x}_{\text{train}})^T \mathbf{w} / \text{sum}(\mathbf{w})$ 
         $error \leftarrow error + (x_{\text{validation}} - \hat{x})^2$ 
      end for
       $rmse.\text{insert}(error/n)$ 
    end for
     $k \leftarrow \text{argmin}(rmse)$ 
     $\mathbf{P}_{t,j} \leftarrow \text{power\_values}_k$ 
  end for
end for

```

The distance matrix $\mathbf{D} \in \mathbb{R}^{MN \times n}$, is the collection of

distances of n stations to the centers of the cells in target grid. The power matrix $P \in \mathbb{R}^{T \times d}$, is the collection of p values for each time step and feature. Note that power operation in $\mathbf{d}_{\text{train}}^{-p}$ is elementwise.

After this process we can define our dataset as follows:

$$\mathcal{D} : \{\{\mathbf{X}_i^1, \dots, \mathbf{X}_i^d\}_{i=t-T_{\text{in}}}^t, \{\mathbf{Y}_j\}_{j=t+1}^{t+T_{\text{out}}}\}_{t=T_{\text{in}}}^{L-T_{\text{out}}}$$

where L is the total time step. We divide the data into different batches where each batch is,

$$\mathcal{B}_j = \{\{\mathbf{X}_i^1, \dots, \mathbf{X}_i^d\}_{i=t-T_{\text{in}}}^t, \{\mathbf{Y}_j\}_{j=t+1}^{t+T_{\text{out}}}\}_{t=T_{\text{in}}}^{L-T_{\text{out}}}, \\ j \in \{0, \dots, b\}, t \in \{0, \dots, L\}$$

where b is the batch size and $\mathcal{D} = \cup_{j=0}^b \mathcal{B}_j$, and $\mathcal{B}_i \cap \mathcal{B}_j \neq \emptyset, \forall i \neq j$ since batches can include same elements of the dataset.

Input series have different units and scales, which requires normalization. However, the dataset is massive, and we need high RAM capacity to normalize such a dataset. Thus, we apply min-max normalization to the batches in an adaptive manner:

$$\mathbf{X}^k = \frac{\mathbf{X}^k - \min(\mathbf{X}^k)}{\max(\mathbf{X}^k) - \min(\mathbf{X}^k)}, \\ \mathbf{X}^k = \{\mathbf{X}_1^k, \dots, \mathbf{X}_T^k\}, \mathbf{X}^k \in \mathcal{B}_j, \\ k \in 1, \dots, d, T = T_{\text{in}} + T_{\text{out}}.$$

For each experiment dataset is divided into three as $\mathcal{D}_{\text{test}}$, $\mathcal{D}_{\text{train}}$ and $\mathcal{D}_{\text{validation}}$. In numerical weather prediction the target value, \mathbf{Y}_j is continuous. Thus, our task is regression. In addition since we have targets to every input data, learning is supervised and we suffer mean squared error,

$$\mathcal{L} = \frac{1}{T_{\text{out}}MN} \sum_{t=1}^{T_{\text{out}}} \sum_{k=1}^M \sum_{l=1}^N (\mathbf{y}_{t,k,l} - \hat{\mathbf{y}}_{t,k,l})^2 \quad (2)$$

where $\hat{\mathbf{y}}$ represents the predicted cell value and \mathbf{y} is the ground truth. Loss function is optimized with Adam [50] using batches of training data.

III. THE WEATHER MODEL

In this section, we describe the developed model architecture of the weather model by referring to every step and formulation shown in Figure 1.

A. Insights into Convolutional LSTMs

One of the key temporal modelling elements in deep learning is the RNN [51]. RNNs carry information through time steps in their memory i.e. the hidden state. This allows RNNs to store temporal information between samples of the input sequence and make them successful in time series prediction tasks. An RNN unit consists of a hidden state \mathbf{h} and an output \mathbf{y} , which operates on variable length data sequence $\mathbf{x} = (\mathbf{x}_1, \dots, \mathbf{x}_T)$, $\mathbf{x}_t \in \mathbb{R}^d$ where T, d refers to temporal window [52] and dimension of inputs respectively. At each time step t , the hidden state is updated by,

$$\mathbf{h}_t = f(\mathbf{h}_{t-1}, \mathbf{x}_t)$$

where f is an non-linear activation function e.g \tanh or σ . For the same input \mathbf{x} , an Elman Network [51] update equations are as follows:

$$\mathbf{h}_t = f_h(\mathbf{W}_h \mathbf{x}_t + U_h \mathbf{h}_{t-1} + b_h), \\ \mathbf{y}_t = f_y(\mathbf{W}_y \mathbf{h}_t + b_y)$$

where $\mathbf{W}_y, \mathbf{W}_h, b_h$ and b_y represent training weights of the network and f_h, f_y are the non-linear activation functions. Since RNNs have only one state \mathbf{h}_t to store the temporal information, they have difficulty of capturing long term dependencies [53]. Moreover, RNNs suffer from vanishing gradients problem [17].

To remedy the problems of RNNs, LSTMs are introduced [53], which are more successful in modeling long term dependencies. A standard fully connected LSTM has a memory cell, which accumulates the state information \mathbf{s}_t that is updated every time step t . At every new input, the cell is updated by three sigmoid gates; the forget gate \mathbf{f}_t , the input gate \mathbf{i}_t and the output gate \mathbf{o}_t . If the input gate is activated, then the input will be accumulated into the cell. If the forget gate is activated, the past cell status \mathbf{s}_{t-1} will be forgotten. The output gate controls whether the cell output \mathbf{s}_t will be propagated to the final state \mathbf{h}_t [7]. The cell state allows to keep the gradient in the cell and preserve the long-term dependencies. The update equations for the gates in LSTM are as follows:

$$\mathbf{i}_t = \sigma(\mathbf{W}_i[\mathbf{h}_{t-1}; \mathbf{x}_t] + \mathbf{b}_i), \\ \mathbf{f}_t = \sigma(\mathbf{W}_f[\mathbf{h}_{t-1}; \mathbf{x}_t] + \mathbf{b}_f), \\ \mathbf{o}_t = \sigma(\mathbf{W}_o[\mathbf{h}_{t-1}; \mathbf{x}_t] + \mathbf{b}_o), \\ \tilde{\mathbf{s}}_t = \tanh(\mathbf{W}_s[\mathbf{h}_{t-1}; \mathbf{x}_t] + \mathbf{b}_s), \\ \mathbf{s}_t = \mathbf{f}_t \odot \mathbf{s}_{t-1} + \mathbf{i}_t \odot \tilde{\mathbf{s}}_t, \\ \mathbf{h}_t = \mathbf{o}_t \odot \tanh(\mathbf{s}_t)$$

where σ and \odot are logistic sigmoid function and elementwise multiplication respectively.

ConvLSTM improves this setup by introducing convolutions to the input-to-state and the state-to-state transitions and captures spatial correlations. Each ConvLSTM unit has inputs $\mathbf{X}_1, \dots, \mathbf{X}_t$, cell outputs $\mathbf{S}_1, \dots, \mathbf{S}_t$, hidden states $\mathbf{H}_1, \dots, \mathbf{H}_t$ and gates $\mathbf{i}_t, \mathbf{f}_t, \mathbf{o}_t$ in 3D tensor format. The update equations for the gates in ConvLSTM are as follows:

$$\mathbf{i}_t = \sigma(\mathbf{W}_{xi} * \mathbf{X}_t + \mathbf{W}_{hi} * \mathbf{H}_{t-1} + \mathbf{b}_i), \\ \mathbf{f}_t = \sigma(\mathbf{W}_{xf} * \mathbf{X}_t + \mathbf{W}_{hf} * \mathbf{H}_{t-1} + \mathbf{b}_f), \\ \mathbf{o}_t = \sigma(\mathbf{W}_{xo} * \mathbf{X}_t + \mathbf{W}_{ho} * \mathbf{H}_{t-1} + \mathbf{b}_o), \\ \tilde{\mathbf{S}}_t = \tanh(\mathbf{W}_{xs} * \mathbf{X}_t + \mathbf{W}_{hs} * \mathbf{H}_{t-1} + \mathbf{b}_s), \\ \mathbf{S}_t = \mathbf{f}_t \odot \mathbf{S}_{t-1} + \mathbf{i}_t \odot \tilde{\mathbf{S}}_t, \\ \mathbf{H}_t = \mathbf{o}_t \odot \tanh(\mathbf{S}_t)$$

where $*$ is the 2D convolution operator. Recall that the input $\mathbf{X}_t \in \mathbb{R}^{M \times N \times n}$ and $\mathbf{H}_t, \mathbf{S}_t \in \mathbb{R}^{M \times N \times m}$ where m equals to the number of hidden dimension. $\mathbf{W}_x, \mathbf{W}_h \in \mathbb{R}^{M \times N}$ and $\mathbf{b}_i, \mathbf{b}_f, \mathbf{b}_o \in \mathbb{R}^{M \times N}$ are the parameters to learn and M, N are the height and width of the filters respectively.

States in the ConvLSTM are the hidden representation of moving objects, where the kernels of ConvLSTM capture these

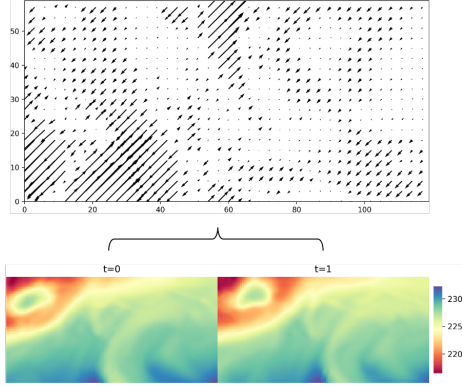


Fig. 3: We obtained flow vectors from two consecutive inputs. The top image shows the magnified version of the flow matrix, which is obtained by the transitions from $t = 0$ to $t = 1$

movements [7]. We observe these movements in the weather features as well. For a target grid $\mathbf{Y}_t \in \mathbb{R}^{M \times N}$ we define the following matrices $\{\mathbf{A}_{t-1}, \mathbf{B}_{t-1}, \mathbf{C}_{t-1}, \mathbf{D}_{t-1}\} \in \mathbb{R}^{M-2 \times N-2}$ for t ,

$$\begin{aligned}\mathbf{A}_{k,l} &= \mathbf{Y}_{i,j} \quad k = 0, \dots, i-2, \quad l = 1, \dots, j-1 \\ \mathbf{B}_{k,l} &= \mathbf{Y}_{i,j} \quad k = 2, \dots, i, \quad l = 1, \dots, j-1 \\ \mathbf{C}_{k,l} &= \mathbf{Y}_{i,j} \quad k = 1, \dots, i-1, \quad l = 0, \dots, j-2 \\ \mathbf{D}_{k,l} &= \mathbf{Y}_{i,j} \quad k = 1, \dots, i-1, \quad l = 2, \dots, j\end{aligned}$$

and we calculate the flow matrix by,

$$\begin{aligned}\mathbf{Y}_t^A &= \mathbf{Y}_t - \mathbf{A}_{t-1} \\ \mathbf{Y}_t^B &= \mathbf{Y}_t - \mathbf{B}_{t-1} \\ \mathbf{Y}_t^C &= \mathbf{Y}_t - \mathbf{C}_{t-1} \\ \mathbf{Y}_t^D &= \mathbf{Y}_t - \mathbf{D}_{t-1} \\ \mathbf{F}_t &= [\mathbf{Y}_t^A + \mathbf{Y}_t^B; \mathbf{Y}_t^C + \mathbf{Y}_t^D]\end{aligned}$$

where the $\mathbf{F}_t \in \mathbb{R}^{M-2 \times N-2 \times 2}$. This means there is a flow vector $\mathbf{f}_t \in \mathbb{R}^2$ for each cell at each time step, t . Figure 3 is an example calculated flow matrix. ConvLSTM learns these flow vectors and passes this information to the next states. However, the traditional side-information integration operations such as creating embeddings using fully connected layers disorient these vectors with non-positive multiplications. Thus, the input to the ConvLSTM structures lost their spatial covariances results with the drastic performance decrease. All in all, the former operations to the inputs of ConvLSTM units must preserve spatial covariances.

B. Encoder and Attention Mechanism

In machine translation [54], [55] proposed the RNN encoder-decoder model. This model can learn a semantically and syntactically meaningful representation of linguistic phrases. The model aims to encode the input sequence to a latent representation and decode into the target sequence. In the early architectures, the encoder-decoder blocks consist of RNNs. An RNN encodes the input sequence into the encoder's hidden state, referring to the previous hidden state. An example

sequence, $\mathbf{x} = (x_1, x_2, \dots, x_T)$ where $\mathbf{x} \in \mathbb{R}^T$, enters the model, and the encoder block learns mapping of

$$\mathbf{h}_t = f(\mathbf{x}, \mathbf{h}_{t-1})$$

where $\mathbf{h}_t \in \mathbb{R}^m$ is the hidden state of the encoder at time t , and m is the size of hidden state. f represents a non-linear function such as RNN, LSTM [53], GRU [56].

In this paper, we use this structure for modelling spatio-temporal sequences. For the n number of spatio-temporal input sequences $\mathbf{X} = (\mathbf{X}_1, \mathbf{X}_2, \dots, \mathbf{X}_T)$ with $\mathbf{X}_t \in \mathbb{R}^{M \times N \times n}$, the encoder learns the mapping of,

$$\mathbf{H}_t = f(\mathbf{X}_t, \mathbf{H}_{t-1})$$

where $\mathbf{H}_t \in \mathbb{R}^{M \times N \times m}$ is the hidden state of the encoder at time t , and m is the size of hidden state. f represents the ConvLSTM units. We show the unrolled view of the encoder in Figure 4. Output of the attention mechanism $\tilde{\mathbf{X}} = (\tilde{\mathbf{X}}_{t-T_{in}}, \dots, \tilde{\mathbf{X}}_t)$ passes to the ConvLSTM units in each layer of the encoder. The layers of the encoder is shown in Figure 1. Each layer encodes the input spatio-temporal series referring to the hidden state on the previous time step. As shown in Figure 1, after the input layer, the hidden layers take the previous layer's outputs as input to their ConvLSTM unit. Each layer has unique hidden states $\mathbf{H}_t^k, \mathbf{S}_t^k$ where k represents the layer index. After every sample the input sequence passed i.e. $t > T_{in}$, the hidden states in every layer, $\mathbf{H}_t^k, \mathbf{S}_t^k$ pass to the context matcher mechanism, and the encoding operation finishes.

We adapt the attention mechanism in [17] and [45] to the spatio-temporal domain. This mechanism aims to extract relevant spatio-temporal series at each time step by referring to the previous encoder's hidden state. As shown in Figure 1, for each time step t , the attention mechanism takes input features of the spatio-temporal time series $\mathbf{X} = \{\{\mathbf{X}_t^i\}_{t=1}^d\}_{i=1}^d$, and the encoder's first layer of the previous hidden state \mathbf{H}_{t-1}^1 to calculate the energy matrices for each $i = 1, \dots, d$,

$$\mathbf{E}^i = \mathbf{V}_E * \tanh(\mathbf{W}_E * \mathbf{H}_{t-1}^1 + \mathbf{U}_E * \mathbf{X}^i) \quad (3)$$

$$\mathbf{A}_{k,l}^i = p(att_{k,l} | \mathbf{X}^i, \mathbf{H}_{t-1}^1) = \frac{\exp(\mathbf{E}_{k,l}^i)}{\sum_k^M \sum_l^N \exp(\mathbf{E}_{k,l}^i)} \quad (4)$$

$$\tilde{\mathbf{X}}_t = \mathbf{A} \odot \mathbf{X}_t \quad (5)$$

where $\mathbf{A} \in \mathbb{R}^{M \times N \times d}$, $\mathbf{E}^i \in \mathbb{R}^{M \times N \times 1}$, $\mathbf{X}^i \in \mathbb{R}^{T \times M \times N}$,

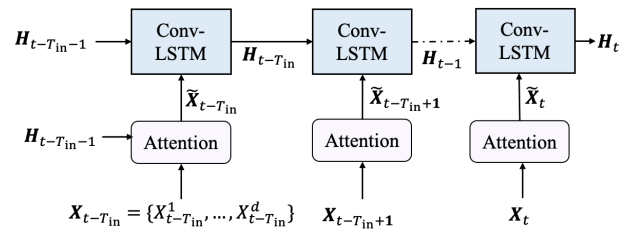


Fig. 4: Input sequence first passes to the attention mechanism and then to the ConvLSTM units, which encode the input spatio-temporal sequence. We represented both hidden states as \mathbf{H}_t .

and $\mathbf{X}_t \in \mathbb{R}^{M \times N \times d}$. Note that the convolution operations in equation 3 are in 2D, where $\mathbf{W}_E \in \mathbb{R}^{K \times K \times m \times Q}$, $\mathbf{U}_E \in \mathbb{R}^{K \times K \times d \times Q}$, $\mathbf{V}_E \in \mathbb{R}^{K \times K \times Q \times 1}$. Here m , d , Q , K specify, hidden, input, attention and kernel dimension numbers respectively. As shown in Figure 1, after performing the convolutions, we obtain the 2D energy matrices for each feature, and we calculate the attention matrix with *softmax* operation in feature dimension as shown in equation 4. Each cell in the \mathbf{A} represents the attention amount given to each of that particular cell's features. The final operation is the Hadamard product of the attention matrix with the input time series, as shown in equation 5. Then, the encoder mapping becomes,

$$\mathbf{H}_t = f(\mathbf{X}_t, \mathbf{H}_{t-1}) \quad (6)$$

where \mathbf{H}_t represents all the hidden states in the encoder layers at t . With the attention mechanism, the encoder can selectively focus on the different spatio-temporal series at each time step by referring to the previous encoder’s hidden state. The critical point in this mechanism is the *softmax* function being non-negative. When we multiply the attention matrix with the input series, we do not change orientations of the flow matrices since the operation is scalar. Thus, we preserve the nature of the input series. Moreover, we used the convolutional operations in the mechanism because the fully-connected methods require taking 2D inputs. If we flattened the input tensor, we would have lost the spatial covariances, and it would be much more costly than the convolutions.

C. Decoder and Context Matcher Mechanism

The purpose of the decoder is to decode the encoded information. As shown in Figure 1, the decoder consists of stacked ConvLSTM units same as the encoder. To prevent performance loss on long length inputs, we introduce a context matcher mechanism. This mechanism sums the hidden states, \mathbf{H}_t^k of the encoder’s layers in time dimension. This way, we can increase the length of gradient flow up to the first time step. As observed in [21], [57], the reversed matching of the hidden states of the encoder’s layers increased the performance. As shown in Figure 1, we used that symmetry in our architecture, and we set the number of layers in the encoder and the decoder the same. The encoder’s hidden state dimensions decrease as the number of layers increases, naturally vice-versa for the decoder. With this architecture, we obey the encoder-decoder design convention, encoding to dense decoding to extend the representation. We can describe context matcher mechanism as,

$$\mathbf{D}_t^{K-k+1} = \sum_{i=t-T_{\text{in}}}^t \mathbf{H}_i^k$$

where $\mathbf{D}_t^{K-k+1} \in \mathbb{R}^{M \times N \times m}$ is the decoder hidden state, K is the total number of layers, and $k \in \{1, \dots, K\}$. As shown in Figure 1, the context matcher sums the hidden states in the time dimension and reverses the order of the states. Next, these states pass to the decoder's corresponding layers, and the input passes the first layer of the decoder. The first layer produces the next hidden state and the input to the next layer.

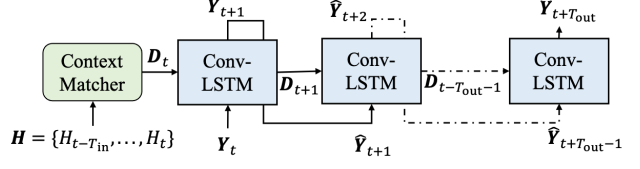


Fig. 5: After the context matcher feeds the initial states, the decoder takes \mathbf{Y}_t as the input to predict $\hat{\mathbf{Y}}_{t+1}$ as the output. Next, the decoder uses this prediction and \mathbf{D}_{t+1} to predict the next output. This process continues until $t = T_{\text{out}}$. We represented both hidden states as \mathbf{D}_t .

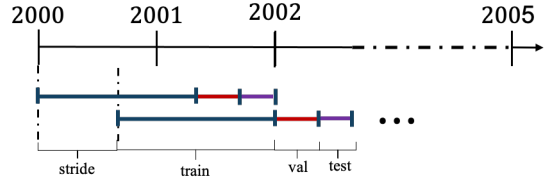


Fig. 6: We show the online training for the experiments between 2000 - 2005. For each experiment, we select two years of data, where the stride is 6 month. We split each selection with 80% of training, 10% of validation, and 10% of test data.

The decoder's final layer produces the inputs to the output convolutions, as shown in Figure 1. Output convolutions allow us to use higher dimensions in the first layer of the encoder. With this layer, we can produce predictions with the desired number of dimensions.

We show the recursive prediction of the decoder in Figure 5. The decoder uses the predictions produced in the previous time step. Thus, we can make any sequence length of predictions with this set-up. We observed that this architecture prevents overfit and increases generalization.

IV. EXPERIMENTS

In this section, we compare our model performance with the baseline models on real weather dataset. We have selected the ConvLSTM, UNet [58], Moving Average as our baseline models. We first described the online training process and our pipeline. Then, we introduced weather dataset with exploratory data analysis to describe our properties of the dataset and select parameters of our model. Finally, we perform the experiments and interpret the results of our attention matrices.

A. The Online Training and Pipeline

We have performed online training since it requires smaller data storage, speeds up the learning, and adapts better for the new data changes. As shown in Figure 6, we have selected two years of period for each experiment and shifted the start date of our period with the stride amount to run the next experiment. In each period we split the data into three sets; train, validation, and test. We have selected the length of period as two years to observe the seasonality, and the stride is six months to make validation and testing in both warm and cold weathers. Totally we have run 10 experiments.

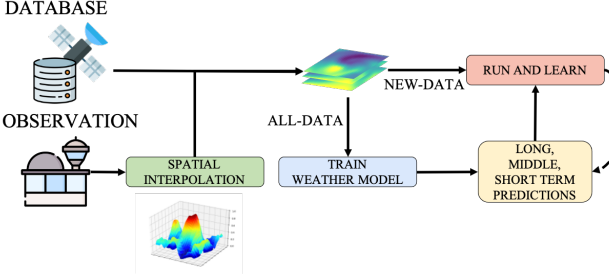


Fig. 7: There are two data sources: the data centers in the grid format and the other from the meteorological stations in time-series format. After spatial interpolation of observations, we train the model and make short-middle-long term predictions. As the new data come, we update the model to make new predictions.

In training, we collected the pieces of batches randomly. The temporal length of each piece is the sum of input and output window sizes. We took samples of this length from the beginning of the set and shifted one time-step in each selection. After covering the whole set, we have shuffled the choices and group them into batches. With this method, we increased the performance of our models.

Note that online training is crucial to assess the performance of the prediction algorithms in real-life applications. We show our pipeline in Figure 7. As the new data comes, we update the model with the online training manner. We make the new short-middle-long term predictions using the model, which has the closest training date to the current date. With this pipeline, we combine the information coming from stations and the database.

B. The Weather Dataset

To compare our model with the baseline models and the literature results, e.g., [47] we have used the benchmark dataset, *ERA5 hourly data on pressure levels* [48]. Temporal resolution of the data is one hour while the spatial resolution is thirty kilometers, and the data belongs to 100 hPa atm pressure level. All in all, our data is in (61×121) shape for each time step and feature. Our data belongs to dates between 2000 and 2005 and spatial covers in latitude $30^\circ - 45^\circ$ and longitude $20^\circ - 50^\circ$. The features belongs to the data is shown in table I. There are many parameters in the ECMWF's database. We have selected these parameters because of the availability and their distribution in time. Some of the parameters we choose did not include many zeros or possess a high percentage of the same value. Among these parameters, we have selected the temperature as our target. Thus, our task is to find the next temperature values using the previous values of the weather features.

We calculated the correlation matrix as shown in Figure 8. According to this matrix we can see strong relations between the features. For example, the temperature is strongly correlated with the geopotential and specific humidity while negatively correlated with relative humidity.

	Units
Geopotential	m^2s^{-2}
Potential vor-	$\text{Km}^2\text{kg}^{-1}\text{s}^{-1}$
ticity	
Relative	%
humidity	
Specific	kg kg^{-1}
humidity	
Temperature	K
U-wind	ms^{-1}
V-wind	ms^{-1}
Verticle Veloc-	Pa s^{-1}
ity	

TABLE I: The corresponding units of the features in ERA5 dataset.

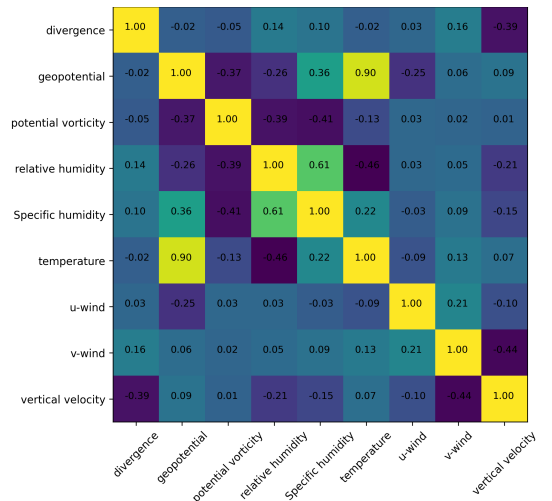


Fig. 8: The shown matrix is the mean of the correlation matrices calculated in each of the target grid's cells. The temporal length of the cells is two years

We performed temporal trend analysis on our data, as shown in Figure 9. For a randomly selected cell, we compare the temperature's shifted values, where we aim to find temporal relations between one day, week, and the previous month's value and current value of the temperature. However, we could not find any consistent relationship, and we can see that the temperature value highly fluctuates. Even though we observe intersections with the shifted values, this rarely happens in one week and one month shifted graphs, and the difference between shifted and current value is significant. When we look at the first time shift in Figure 9a, we observe steeps and valleys where the previous temperature values are close. We can conclude that the next value at most depends on the ten last time step. After ten time steps, it highly varies. To this end, we have selected 10 time steps of input data and try to predict 10 time step ahead. Furthermore, when we look at Figure 9d, we observe a seasonal trend in the series. Thus, in our experiments, we selected the temporal length at least two years to learn the data's seasonality.

The other parameters of the *Weather Model* is as follows:

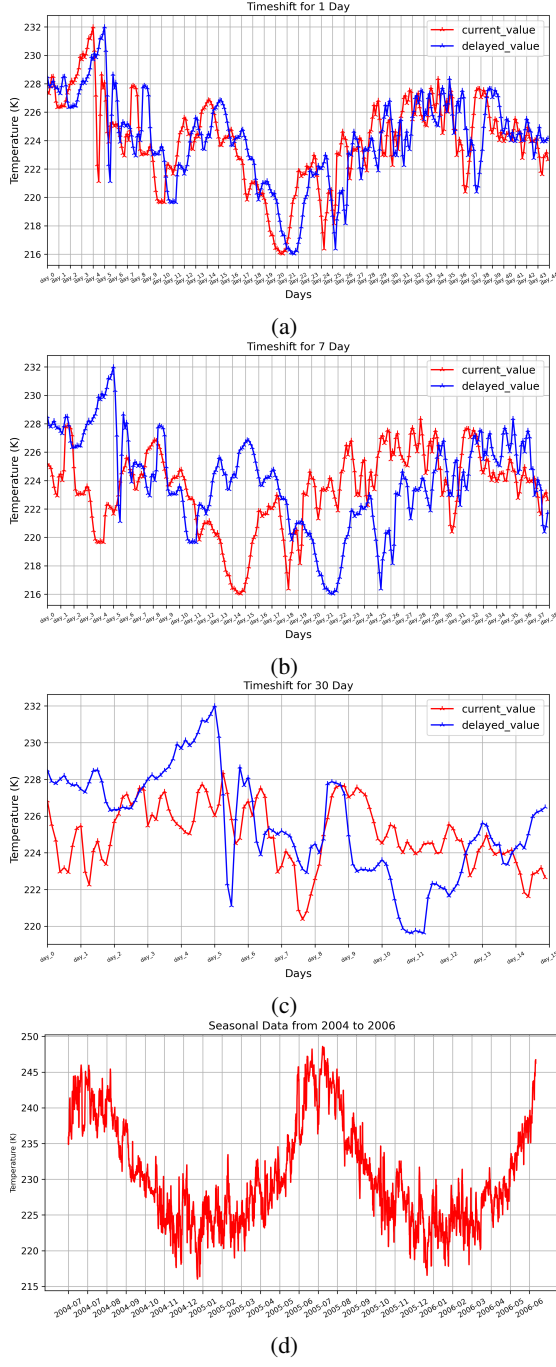


Fig. 9: We show the temporal trend of temperature. (a) shows the comparison of the current value with one day shift, (b) for one week shift, and (c) for one month shift. (d) shows the seasonal trend of the data from 2004 to 2006. These temporal graphs belong to a randomly selected cell.

There are three layers of ConvLSTM units in the encoder and the decoder. The hidden dimensions of the encoder is 32, 32, 16 and for the decoder 16, 32, 32. The kernel sizes of the layers in the encoder are 5, 3, 1, and the decoder 3, 3, 1. We set the hidden states to zero at the beginning of each epoch. Next, we select the attention dimension as 5, where the kernel sizes of the convolutions are 3. Lastly, there are two layers of convolution units at the end of the decoder's last layer, where

the middle channel is 5, and the output channel is 1. Below, we describe the parameters of baseline models.

C. The Baseline Models

We find the best parameters of all the models using grid-search. After 4 consecutive validation loss increment the training stops and saves the best model, which has the smallest validation loss.

1) *Simple Moving Average (SMA)*: In this model, the estimate at time t is obtained by averaging values of the input spatio-temporal series within k periods of t where k is the window length [59]. The model has a temporal mask called the window. Input window length equals to T_{in} and we selected as $T_{in} = 30$. Moreover, the model provides recurrent predictions, which means, after the first prediction, $t = T_{in} + 1$, the predicted value is inserted to the end of the input values to provide the next prediction. This process repeats T_{out} times and produce the output sequence. In this paper, unlike SMA, we train the input window. We initialize the weights with a uniform random variable where the range is $[0, 1]$. At every time step, we suffer the square loss given in (2), and train the weights of the input window using Stochastic Gradient Descent (SGD).

2) *U-net*: We have implemented the model architecture introduced in [58]. Model takes 10 steps of temperature spatio-temporal series and predict 10 steps ahead. The architecture consists of 4 downsample and 4 upsample layers. We suffer the square loss given in (2), and train the model with Adam optimizer.

3) *ConvLSTM*: The model's architecture in experiments is the same as the forecasting network proposed in [7]. However, there are some differences, which improved the performance of this model. Since the reversing of the encoder's hidden states enhances the performance of ConvLSTM architectures, we used that method in this model. The encoder consists of three layers of ConvLSTM units. 1, 16, 32 are the number of hidden dimensions in each encoder layer, and 5, 3, 1 are the kernel sizes. ConvLSTM units have the same number of hidden dimensions and kernel sizes in each layer of the decoder with reverse order of these series. We set the hidden states to zero at the beginning of each epoch, and the decoder takes zero tensors as input. To prevent exploding gradient problems in LSTM based architectures, we select the clip parameter as 5.

D. Performance Analysis and Results

We perform our experiments on our dataset with three hours of frequency, which means eight time-steps belong to the same day. We compare the performance of all models by square loss given in (2). We show the results of our experiments in Table II, the learning curves belong to these experiment are in Appendix-B. Our model obtains the best validation and the best test score, which shows that our model generalizes the data better. Moreover, we observe that the U-Net and the ConvLSTM models have a high-performance gap between validation and test scores, caused by overfitting to the training data.

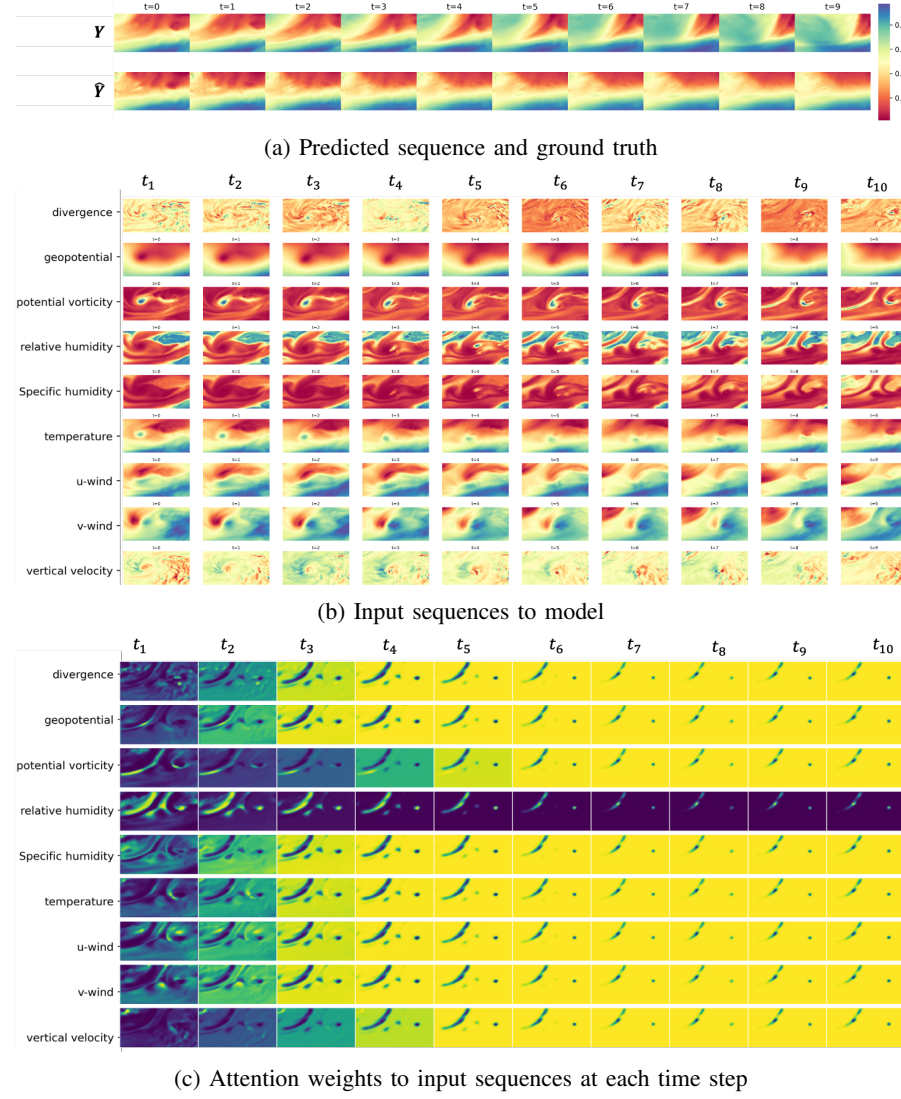


Fig. 10: We show the *Weather Model* result with the input sequence, output sequence, and attention weights at each time step. Observe the cyclone in the input sequence's features; potential vorticity, relative-specific humidity, and temperature. Towards the first time steps, the model focuses on the stationary parts in the input sequences. Towards the end of the series, other than the relative humidity most of the attention weights converge to 1 since most of these stationary parts fade away. The model needs every movement in the last time-steps since they are very close to the current values. Besides, note that the inverse attention weight relation between the relative humidity and the temperature features. We have shown in Figure 8 they are inversely correlated.

In addition, we observe a fluctuation on the test and validation scores in every model. Since we shift the experiment range by six months, we select the validation and test scores from winter season to summer season. Since there are more weather events happen during winter time, the movements of the weather are less predictable. Thus, there is a performance decrease during winter season in every model.

To analyze the model's spatial and temporal performance, we show the predicted sequence's heat maps with the ground truth in Figure 10a. When we examine the graph, we can say our model can learn temperature fluctuations in time. Naturally, the performance of our model deteriorates as the length of the prediction interval increases. However, when compared with the ground truth, our model successfully generalizes the

fluctuations in temperature. Moreover, when we compare our model with the baseline models in Appendix-A; between time steps, we observe that our model can represent the formation of temperature waves and free from making constant predictions.

We show the multiple spatio-temporal series inputs in Figure 10b. We can realize that a cyclone or swirl of winds located at the center of the data. After ten time-step, this cyclone fades away, and another one occurs in other location. Figure 10c shows that our model focuses on these areas with different attention weights in various features. We observe that these weights show the same correlation pattern in the Figure 8. However, towards the current time step, i.e. t_{10} weights becomes less distinctive and converge to one caused by the fading of cyclone and the data's temporal trend, as we men-

Validation Scores				
Experiment	SMA	U-Net	ConvLSTM	Weather Model
1	2.4	2.11	1.7	1.18
2	7.13	4.41	3.32	3.08
3	3.89	1.85	1.8	1.57
4	5.48	3.06	2.49	2.11
5	2.72	2.19	1.75	1.43
6	4.41	2.29	3.42	2.19
7	2.58	1.53	1.42	0.96
8	3.30	2.59	1.75	1.95
9	3.85	1.88	1.71	1.45
10	5.48	2.35	2.72	1.75
Test Scores				
Experiment	SMA	U-Net	ConvLSTM	Weather Model
1	4.44	3.77	3.54	2.33
2	4.83	3.39	2.29	2.04
3	6.36	3.02	2.92	2.47
4	3.26	2.34	1.46	1.32
5	5.05	3.22	2.91	2.40
6	3.21	1.77	2.67	1.76
7	5.38	2.96	2.76	1.77
8	4.12	2.68	1.93	2.11
9	5.49	2.87	2.37	2.05
10	3.42	1.91	1.85	1.38

TABLE II: We show model’s validation and test MSE scores. Bold scores are the lowest.

tioned in Section-III-B. Considering the current temperature values are positively correlated with the early pasted values, the model needs to focus on every input data movement. Thus, the attention matrices converge to 1 towards the end of input data series.

V. CONCLUSION

We studied spatio-temporal weather data and incorporated the observations to perform weather forecasting with a deep learning pipeline. We introduced a novel ConvLSTM network structure with attention and context matcher mechanism to extend the encoder-decoder method. The model jointly trains both attention weights and ConvLSTM units. Moreover, we provided the problem as a spatio-temporal sequence prediction problem with multiple sources of information and implemented a spatial interpolation algorithm. We analytically showed our objective function and preprocessing steps. We show that, we can learn spatial-temporal correlations with the introduced model and provide predictions using multiple spatio-temporal series with high interpretability.

Furthermore, by giving the innate nature of the input spatio-temporal series with flow vectors, we explained incorrect side-information integration to ConvLSTM networks in the literature. Then, we analyzed our network’s performance with real-life datasets, which have high spatial and temporal resolution. In our experiments, by providing quantitative and qualitative comparisons between the predicted and the ground truth

values, we evaluated our model’s performance in temporal and spatial dimensions. Our model can learn the formation and decay movements of temperature waves. We observe that our model shows significant performance gains compared to the baseline models in our experiments.

REFERENCES

- [1] G. Luo, S. Yang, G. Tian, C. Yuan, W. Hu, and S. J. Maybank, “Learning human actions by combining global dynamics and local appearance,” *IEEE Transactions on Pattern Analysis and Machine Intelligence*, vol. 36, no. 12, pp. 2466–2482, 2014.
- [2] L. Kratz and K. Nishino, “Tracking pedestrians using local spatio-temporal motion patterns in extremely crowded scenes,” *IEEE Transactions on Pattern Analysis and Machine Intelligence*, vol. 34, no. 5, pp. 987–1002, 2012.
- [3] B. Barz, E. Rodner, Y. G. Garcia, and J. Denzler, “Detecting regions of maximal divergence for spatio-temporal anomaly detection,” *IEEE Transactions on Pattern Analysis and Machine Intelligence*, vol. 41, no. 5, pp. 1088–1101, 2019.
- [4] F. Zhou and F. De la Torre, “Spatio-temporal matching for human pose estimation in video,” *IEEE Transactions on Pattern Analysis and Machine Intelligence*, vol. 38, no. 8, pp. 1492–1504, 2016.
- [5] M. Demirkus, D. Precup, J. J. Clark, and T. Arbel, “Hierarchical spatio-temporal probabilistic graphical model with multiple feature fusion for binary facial attribute classification in real-world face videos,” *IEEE Transactions on Pattern Analysis and Machine Intelligence*, vol. 38, no. 6, pp. 1185–1203, 2016.
- [6] J. Liu, A. Shahroudy, D. Xu, A. C. Kot, and G. Wang, “Skeleton-based action recognition using spatio-temporal lstm network with trust gates,” *IEEE Transactions on Pattern Analysis and Machine Intelligence*, vol. 40, no. 12, pp. 3007–3021, 2018.
- [7] S. Xingjian, Z. Chen, H. Wang, D.-Y. Yeung, W.-K. Wong, and W.-c. Woo, “Convolutional lstm network: A machine learning approach for precipitation nowcasting,” in *Advances in neural information processing systems*, 2015, pp. 802–810.
- [8] C. Abbe, “The physical basis of long-range weather forecasts,” *Monthly Weather Review*, vol. 29, no. 12, pp. 551–561, 1901.
- [9] E. R. Rodrigues, I. Oliveira, R. Cunha, and M. Netto, “DeepDownscale: A deep learning strategy for high-resolution weather forecast,” *Proceedings - IEEE 14th International Conference on eScience, e-Science 2018*, pp. 415–422, 2018.
- [10] J. G. Powers, J. B. Klemp, W. C. Skamarock, C. A. Davis, J. Dudhia, D. O. Gill, J. L. Coen, D. J. Gochis, R. Ahmadov, S. E. Peckham *et al.*, “The weather research and forecasting model: Overview, system efforts, and future directions,” *Bulletin of the American Meteorological Society*, vol. 98, no. 8, pp. 1717–1737, 2017.
- [11] F. Molteni, R. Buizza, T. N. Palmer, and T. Petrolia, “The ecmwf ensemble prediction system: Methodology and validation,” *Quarterly journal of the royal meteorological society*, vol. 122, no. 529, pp. 73–119, 1996.
- [12] M. Déqué, C. Dreveton, A. Braun, and D. Cariolle, “The arpege/ifs atmosphere model: a contribution to the french community climate modelling,” *Climate Dynamics*, vol. 10, no. 4–5, pp. 249–266, 1994.
- [13] P. Termonia, C. Fischer, E. Bazile, F. Bouyssel, R. Brožková, P. Bénard, B. Bochenek, D. Degrauwe, M. Derkoviá, R. El Khatib *et al.*, “The aladin system and its canonical model configurations aroma cy41t1 and alaro cy40t1,” *Geoscientific Model Development*, vol. 11, pp. 257–281, 2018.
- [14] I. Dimoulkas, P. Mazidi, and L. Herre, “Neural networks for GEFCom2017 probabilistic load forecasting,” *International Journal of Forecasting*, vol. 35, no. 4, pp. 1409–1423, 2019. [Online]. Available: <https://doi.org/10.1016/j.ijforecast.2018.09.007>
- [15] M. Cai, M. Pipattanasomporn, and S. Rahman, “Day-ahead building-level load forecasts using deep learning vs. traditional time-series techniques,” *Applied Energy*, vol. 236, no. October 2018, pp. 1078–1088, 2019. [Online]. Available: <https://doi.org/10.1016/j.apenergy.2018.12.042>
- [16] S. Smil, “A hybrid method of exponential smoothing and recurrent neural networks for time series forecasting,” *International Journal of Forecasting*, vol. 36, no. 1, pp. 75–85, 2020. [Online]. Available: <https://doi.org/10.1016/j.ijforecast.2019.03.017>
- [17] Y. Qin, D. Song, H. Chen, W. Cheng, G. Jiang, and G. Cottrell, “A dual-stage attention-based recurrent neural network for time series prediction,” *arXiv preprint arXiv:1704.02971*, 2017.

[18] S. Bai, J. Z. Kolter, and V. Koltun, “An empirical evaluation of generic convolutional and recurrent networks for sequence modeling,” *arXiv*, 2018.

[19] A. van den Oord, S. Dieleman, H. Zen, K. Simonyan, O. Vinyals, A. Graves, N. Kalchbrenner, A. Senior, and K. Kavukcuoglu, “WaveNet: A Generative Model for Raw Audio,” pp. 1–15, 2016. [Online]. Available: <http://arxiv.org/abs/1609.03499>

[20] R. Sen, H. F. Yu, and I. Dhillion, “Think globally, act locally: A deep neural network approach to high-dimensional time series forecasting,” *arXiv*, pp. 1–14, 2019.

[21] X. Shi, Z. Gao, L. Lausen, H. Wang, D.-Y. Yeung, W.-k. Wong, and W.-c. Woo, “Deep learning for precipitation nowcasting: A benchmark and a new model,” in *Advances in neural information processing systems*, 2017, pp. 5617–5627.

[22] S. Agrawal, L. Barrington, C. Bromberg, J. Burge, C. Gazen, and J. Hickey, “Machine learning for precipitation nowcasting from radar images,” *arXiv preprint arXiv:1912.12132*, 2019.

[23] W.-c. Woo and W.-k. Wong, “Operational application of optical flow techniques to radar-based rainfall nowcasting,” *Atmosphere*, vol. 8, no. 3, p. 48, 2017.

[24] H. De Vries, F. Strub, J. Mary, H. Larochelle, O. Pietquin, and A. Courville, “Modulating early visual processing by language,” *Advances in Neural Information Processing Systems*, vol. 2017–December, pp. 6595–6605, 2017.

[25] E. Perez, F. Strub, H. De Vries, V. Dumoulin, and A. Courville, “FiLM: Visual reasoning with a general conditioning layer,” *32nd AAAI Conference on Artificial Intelligence, AAAI 2018*, pp. 3942–3951, 2018.

[26] X. Wang, K. Yu, C. Dong, and C. Change Loy, “Recovering Realistic Texture in Image Super-Resolution by Deep Spatial Feature Transform,” *Proceedings of the IEEE Computer Society Conference on Computer Vision and Pattern Recognition*, pp. 606–615, 2018.

[27] Y. Liang, S. Ke, J. Zhang, X. Yi, and Y. Zheng, “Geoman: Multi-level attention networks for geo-sensory time series prediction,” *IJCAI International Joint Conference on Artificial Intelligence*, vol. 2018–July, pp. 3428–3434, 2018.

[28] J. N. Liu, Y. Hu, Y. He, P. W. Chan, and L. Lai, “Deep neural network modeling for big data weather forecasting,” in *Information Granularity, Big Data, and Computational Intelligence*. Springer, 2015, pp. 389–408.

[29] M. Hossain, B. Rekabdar, S. J. Louis, and S. Dascalu, “Forecasting the weather of Nevada: A deep learning approach,” *Proceedings of the International Joint Conference on Neural Networks*, vol. 2015–September, pp. 2–7, 2015.

[30] A. G. Salman, B. Kanigoro, and Y. Heryadi, “Weather forecasting using deep learning techniques,” *ICACSIS 2015 - 2015 International Conference on Advanced Computer Science and Information Systems, Proceedings*, vol. 00, pp. 281–285, 2016.

[31] J. Lee, C. G. Kim, J. E. Lee, N. W. Kim, and H. Kim, “Application of artificial neural networks to rainfall forecasting in the Geum River Basin, Korea,” *Water (Switzerland)*, vol. 10, no. 10, 2018.

[32] K. Zhou, Y. Zheng, B. Li, W. Dong, and X. Zhang, “Forecasting Different Types of Convective Weather: A Deep Learning Approach,” *Journal of Meteorological Research*, vol. 33, no. 5, pp. 797–809, 2019.

[33] B. Kanigoro and A. G. Salman, “Recurrent gradient descent adaptive learning rate and momentum neural network for rainfall forecasting,” in *2016 international seminar on application for technology of information and communication (ISemantic)*. IEEE, 2016, pp. 23–26.

[34] M. A. Zaytar and C. El Amrani, “Sequence to sequence weather forecasting with long short-term memory recurrent neural networks,” *International Journal of Computer Applications*, vol. 143, no. 11, pp. 7–11, 2016.

[35] S. Poornima and M. Pushpalatha, “Prediction of rainfall using intensified LSTM based recurrent Neural Network with Weighted Linear Units,” *Atmosphere*, vol. 10, no. 11, 2019.

[36] B. Wang, H. Luo, J. Lu, T. Li, G. Zhang, Z. Yan, and Y. Zheng, “Deep uncertainty quantification: A machine learning approach for weather forecasting,” *Proceedings of the ACM SIGKDD International Conference on Knowledge Discovery and Data Mining*, pp. 2087–2095, 2019.

[37] P. Hewage, M. Trovati, E. Pereira, and A. Behera, “Deep learning-based effective fine-grained weather forecasting model,” *Pattern Analysis and Applications*, no. 0123456789, 2020. [Online]. Available: <https://doi.org/10.1007/s10044-020-00898-1>

[38] S. Kim, H. Kim, J. Lee, S. Yoon, S. E. Kahou, K. Kashinath, and Prabhat, “Deep-hurricane-tracker: Tracking and forecasting extreme climate events,” *Proceedings - 2019 IEEE Winter Conference on Applications of Computer Vision, WACV 2019*, pp. 1761–1769, 2019.

[39] Q. K. Tran and S. K. Song, “Computer vision in precipitation nowcasting: Applying image quality assessment metrics for training deep neural networks,” *Atmosphere*, vol. 10, no. 5, pp. 1–20, 2019.

[40] A. Heye, K. Venkatesan, and J. Cain, “Precipitation Nowcasting: Leveraging Deep Recurrent Convolutional Neural Networks,” *Proceedings of the Cray User Group (CUG) 2017*, 2017. [Online]. Available: https://cug.org/proceedings/cug2017/_proceedings/includes/files/pap155s2-file1.pdf

[41] J. R. Jing, Q. Li, X. Y. Ding, N. L. Sun, R. Tang, and Y. L. Cai, “AENN: A GENERATIVE ADVERSARIAL NEURAL NETWORK for WEATHER RADAR ECHO EXTRAPOLATION,” *International Archives of the Photogrammetry, Remote Sensing and Spatial Information Sciences - ISPRS Archives*, vol. 42, no. 3/W9, pp. 89–94, 2019.

[42] S. Agrawal, L. Barrington, C. Bromberg, J. Burge, C. Gazen, and J. Hickey, “Machine learning for precipitation nowcasting from radar images,” *arXiv*, no. NeurIPS, pp. 1–6, 2019.

[43] S. Song, C. Lan, J. Xing, W. Zeng, and J. Liu, “An end-to-end spatio-temporal attention model for human action recognition from skeleton data,” *31st AAAI Conference on Artificial Intelligence, AAAI 2017*, pp. 4263–4270, 2017.

[44] H. Yao, X. Tang, H. Wei, G. Zheng, and Z. Li, “Revisiting spatial-temporal similarity: A deep learning framework for traffic prediction,” *33rd AAAI Conference on Artificial Intelligence, AAAI 2019, 31st Innovative Applications of Artificial Intelligence Conference, IAAI 2019 and the 9th AAAI Symposium on Educational Advances in Artificial Intelligence, EAAI 2019*, pp. 5668–5675, 2019.

[45] L. Zhang, L. Mei, S. A. A. Shah, G. Zhu, P. Shen, and M. Bennamoun, “Attention in convolutional LSTM for gesture recognition,” *Advances in Neural Information Processing Systems*, vol. 2018–December, no. NeurIPS, pp. 1953–1962, 2018.

[46] I. A. Abdellaoui and S. Mehrkanoon, “Deep multi-stations weather forecasting: explainable recurrent convolutional neural networks,” 2020. [Online]. Available: <http://arxiv.org/abs/2009.11239>

[47] S. Rasp, P. D. Dueben, S. Scher, J. A. Weyn, S. Mouatadid, and N. Thuerer, “WeatherBench: A Benchmark Data Set for Data-Driven Weather Forecasting,” *Journal of Advances in Modeling Earth Systems*, vol. 12, no. 11, 2020.

[48] H. Hersbach, B. Bell, P. Berrisford, S. Hirahara, A. Horányi, J. Muñoz-Sabater, J. Nicolas, C. Peubey, R. Radu, D. Schepers, A. Simmons, C. Soci, S. Abdalla, X. Abellán, G. Balsamo, P. Bechtold, G. Biavati, J. Bidlot, M. Bonavita, G. De Chiara, P. Dahlgren, D. Dee, M. Diamantakis, R. Dragani, J. Flemming, R. Forbes, M. Fuentes, A. Geer, L. Haimberger, S. Healy, R. J. Hogan, E. Hólm, M. Janisková, S. Keeley, P. Laloyaux, P. Lopez, C. Lupu, G. Radnoti, P. de Rosnay, I. Rozum, F. Vamborg, S. Villaume, and J. N. Thépaut, “The ERA5 global reanalysis,” *Quarterly Journal of the Royal Meteorological Society*, 2020.

[49] G. Y. Lu and D. W. Wong, “An adaptive inverse-distance weighting spatial interpolation technique,” *Computers and Geosciences*, 2008.

[50] D. P. Kingma and J. Ba, “Adam: A method for stochastic optimization,” *arXiv preprint arXiv:1412.6980*, 2014.

[51] J. L. Elman, “Finding structure in time,” *Cognitive science*, vol. 14, no. 2, pp. 179–211, 1990.

[52] K. Cho, B. Van Merriënboer, C. Gulcehre, D. Bahdanau, F. Bougares, H. Schwenk, and Y. Bengio, “Learning phrase representations using rnn encoder-decoder for statistical machine translation,” *arXiv preprint arXiv:1406.1078*, 2014.

[53] S. Hochreiter and J. Schmidhuber, “Long short-term memory,” *Neural computation*, vol. 9, no. 8, pp. 1735–1780, 1997.

[54] K. Cho, B. Van Merriënboer, D. Bahdanau, and Y. Bengio, “On the properties of neural machine translation: Encoder-decoder approaches,” *arXiv preprint arXiv:1409.1259*, 2014.

[55] I. Sutskever, O. Vinyals, and Q. V. Le, “Sequence to sequence learning with neural networks,” in *Advances in neural information processing systems*, 2014, pp. 3104–3112.

[56] K. Cho, B. Van Merriënboer, C. Gulcehre, D. Bahdanau, F. Bougares, H. Schwenk, and Y. Bengio, “Learning phrase representations using rnn encoder-decoder for statistical machine translation,” *arXiv preprint arXiv:1406.1078*, 2014.

[57] Q.-K. Tran and S.-k. Song, “Computer vision in precipitation nowcasting: Applying image quality assessment metrics for training deep neural networks,” *Atmosphere*, vol. 10, no. 5, p. 244, 2019.

[58] O. Ronneberger, P. Fischer, and T. Brox, “Unet,” *MICCAI2015*, 2015.

[59] R. J. Hyndman and G. Athanasopoulos, *Forecasting: principles and practice*. OTexts, 2018.

APPENDIX A

THE VISUAL PERFORMANCE COMPARISON OF THE MODELS

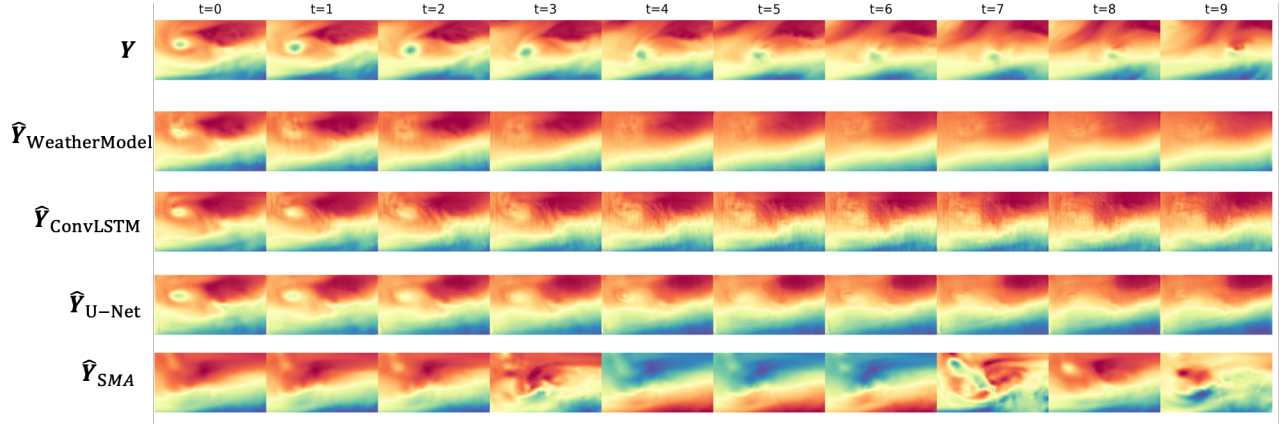


Fig. 11: We show the visual comparison of the models. \mathbf{Y} is the ground truth while $\hat{\mathbf{Y}}$ is the predictions belong to the models.

APPENDIX B

LEARNING CURVES OF THE MODELS

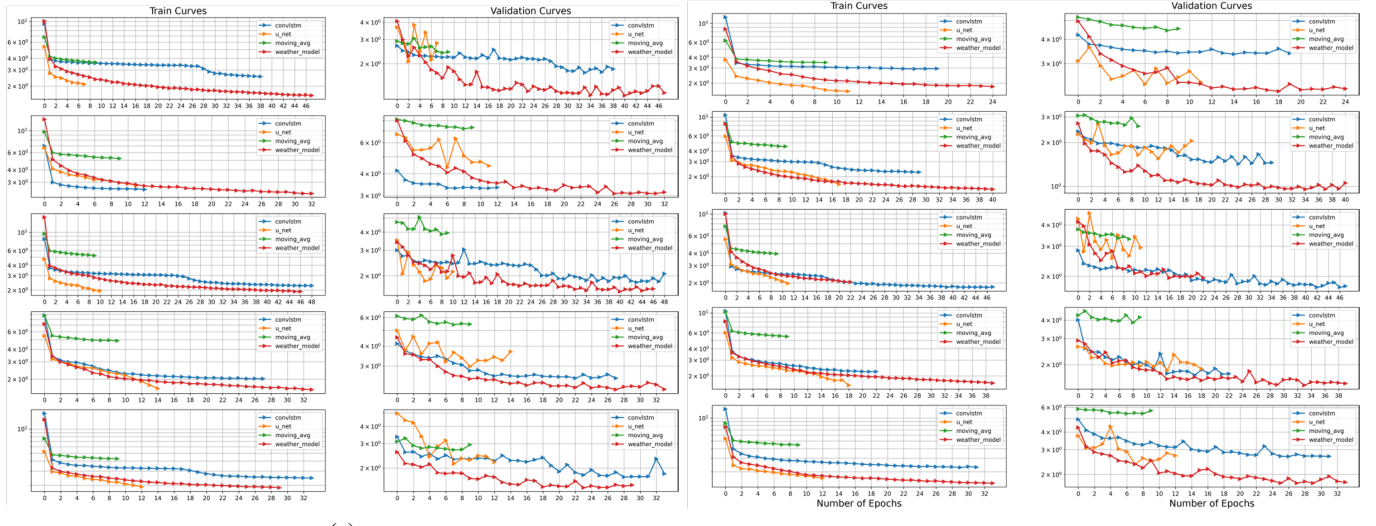


Fig. 12: We show the train and validation curves of each experiment. These curves belong to the test scores of experiments shown in Table II. Figure 12a shows the first five of the experiments while Figure 12b shows the remaining five.